Registration of a priori Information for Computed Laminography

Christian SCHORR [1], Laura DÖRR [1], Michael MAISL [1], Thomas SCHUSTER[2]

[1] Fraunhofer-Institut für Zerstörungsfreie Prüfverfahren IZFP, Campus E3.1, 66123 Saarbrücken, Germany
Phone: +49 681 9302 3935; Fax : +49 681 9302 5901; e-mail: christian.schorr@izfp.fraunhofer.de, laura.doerr@izfp.fraunhofer.de, michael.maisl@izfp.fraunhofer.de
[2]Universität des Saarlandes, Campus E1.1, 66123 Saarbrücken, Germany
Phone: +49 681 302 57425, Fax: +49 681 302 4435; e-mail: thomas.schuster@num.uni-sb.de

Abstract

Reconstructed 3D volumes from computed laminography data suffer from blurring artefacts due to the laminographic geometry. Such losses in quality can be compensated for by integrating a priori information about the test object into the iterative reconstruction process. However, this requires the position of the a priori model to be fitted exactly to the measured data. A (semi-)automatic 2D-3D registration algorithm which only requires a minimal additional user input and is based on a mathematical optimization problem is presented. Using measurement data obtained by simulating X-ray projections of the laminographic scanner CLARA the algorithm is validated.

Keywords

Registration, computed laminography, iterative reconstruction, a priori information

1. Introduction

Over the last few decades, computed tomography (CT) has become a well-established and widely used method of nondestructive testing.

It allows a 3D analysis of the interior structure of an object using X-rays and mathematical reconstruction algorithms. To this end, the object is placed on a rotation table between an X-ray source and a detector, which provides irradiation images of the object (fig. 1). The object is then rotated by 360° while an entire data set of projections from all angles is obtained. From these images a volume representing the density distribution of the object can be computed using mathematical reconstruction algorithms.

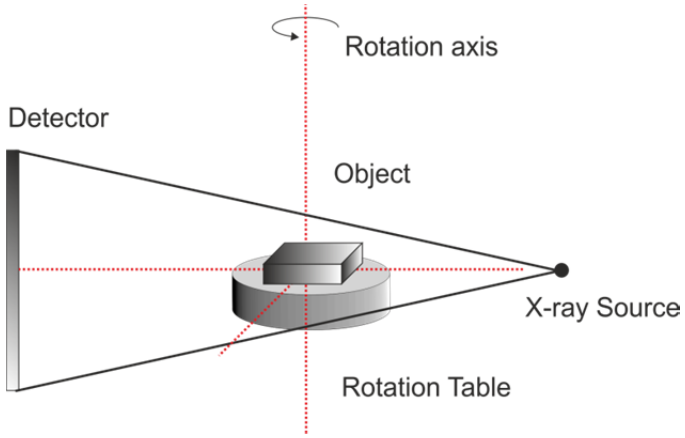

Figure 1. Industrial CT set-up.

Still there are some test cases in which this powerful technique for investigating the test object's inner structure is not applicable. For instance, if a planar object, i.e. a potentially very large but extremely flat object, is to be measured using CT two major problems arise. The first of which is caused by the extreme differences in the object's diameters in longitudinal and transversal direction. As CT relies on a full rotation of 360° the object needs to be penetrated by X-rays from each direction. In order for the X-rays not to be fully attenuated when passing through the object in longitudinal direction, their energy has to be sufficiently high which in turn leads to very weak contrast in transversal directions and may result in unusable measurements. The second problem is encountered when aiming for a high magnification ratio. The latter is increased by reducing the distance between object and X-ray source. Especially for fine-structured planar objects the feasible magnification factor may require the object to be so close to the detector that a full object rotation is no longer possible without causing a collision of object and X-ray tube. Both these problems are solved by computed laminography (CL). Contrary to traditional CT, for this X-ray technique, neither does the axis between source and detector need to be perpendicular to the rotation axis, nor does the rotation performed necessarily need to measure 360°. There are numerous different CL geometries, some relying on linear or planar translations of the components (classical CL), and others representing a tilted version of the traditional CT geometry using a 360° rotation (CLARA) [1] (fig. 2). Using this trajectory, the object can be placed arbitrarily close to the X-ray tube without risking a collision with the latter, thereby enabling an appropriate magnification factor.

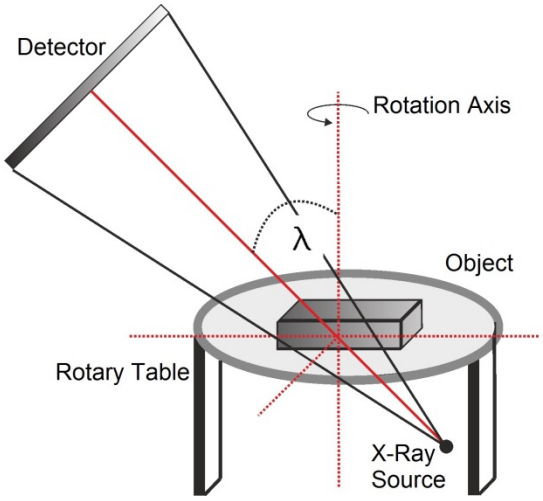

Figure 2. CLARA geometrical composition.

2. A priori Information

While allowing for a high-resolution measurement of planar objects, computed laminography also has some limitations. Most important, the 3D reconstructions computable from CL data exhibit an anisotropic depth resolution in beam direction. In case of the CLARA geometry, this is due to the constrained ray directions which can only

provide limited information. As the (planar) object is always irradiated from the same side, the information gained is not as complete as in a CT where the object can be irradiated from all sides. Therefore, CL reconstructions typically show artefacts and blurring orthogonal to the so-called focus plane which lies normal to the rotation axis. This also results in the fact that the object's density cannot be reconstructed faithfully in an absolute sense but only in a relative way, so that the object's structure is still reconstructed correctly but not with the correct density values. Furthermore, CL data cannot be reconstructed using standard CT algorithms of filtered back projection type like the Feldkamp algorithm [11]. Instead, iterative methods like SART (simultaneous algebraic reconstruction technique) [2] have to be applied. This constitutes an advantage since iterative methods allow the use of geometric a priori information about the object. This prior knowledge may consist of the object's surface given by a mesh model or a CAD (Computer aided design) file. It allows restricting the reconstruction to areas where the a priori information predicts material to be present and avoid reconstructing empty air areas. This greatly reduces the typical laminographic artefacts by forcing them from the air area the into the material area leading to an increased contrast and defect detectability.

The SART algorithm models the measurement process as a system of linear equations and tries to solve it iteratively. Let the 3D volume consisting of n voxels with indices $j = 1, \dots, n$ be described by $f \in \mathbb{R}^n$, the measured rays be given by p_i, $i = 1, \dots, m$ and ω_{ij} correspond to the fraction of the i-th ray p_i passing through pixel j. Then, each SART iteration reads

$$f_j^{(k+1)} = f_j^{(k)} + \lambda \cdot \frac{\sum_{p_i \in P_\alpha} \left(\frac{p_i - \sum_{l=1}^{n} \omega_{il} f_l^{(k)}}{\sum_{l=1}^{n} \omega_{il}} \right)}{\sum_{p_i \in P_\alpha} \omega_{ij}}, \qquad (1)$$

where $\lambda \in \mathbb{R}$ is a relaxation factor, chosen depending on the structure and material composition of the inspected object, and P_α the set of rays belonging to projection $\alpha \in \{\alpha_1, \dots, \alpha_p\}$. A priori information can easily be integrated into this reconstruction process if it is given as a second, binary voxel volume g of the same dimensions as the volume to be reconstructed, i.e. $g_j \in \{0,1\}$ with g_j indicating whether voxel j contains material or not. In this case, the a priori SART iteration step is given by

$$f_j^{(k+1)} = f_j^{(k)} + g_j \cdot \lambda \cdot \frac{\sum_{p_i \in P_\alpha} \left(\frac{p_i - \sum_{l=1}^{n} \omega_{il} f_l^{(k)}}{\sum_{l=1}^{n} \omega_{il}} \right)}{\sum_{p_i \in P_\alpha} \omega_{ij}} \qquad (2)$$

This straight-forward integration of a priori information not only increases the convergence speed of the reconstruction process but at the same time offers the possibility of reducing the blurring artefacts characteristic for computed laminography reconstructions as well as increasing contrast. As a result, defects become more easily detectable [3,4]. As a priori information given CAD or STL (stereolithography) data or data obtained using a different method of nondestructive testing can be used. In most cases, the a priori data available does not coincide with the measured CL data concerning orientation and scale of the test object and therefore cannot be used without prior registration. This implies the need for a preprocessing step determining the transformation which positions the a priori data to properly fit the measured projections.

3. (Semi-)Automatic Registration Algorithm

Image registration has become a growing field of research with new algorithms keeping pace with the development of new imaging techniques and sensor hardware. Besides the traditional challenge of 2D-2D image registration, the ever expanding processing power of modern computers also brings the registration of volumes into focus. An overview of registration methods can be found in [6,8,9]. For our problem the obvious approach of reconstructing the measured CL data to obtain a 3D volume which can be registered to the a priori data of the same dimensionality cannot be pursued as the traditional CL reconstruction is severely degraded by blurring artefacts. Thus, instead of using a 3D-3D registration algorithm, the 2D projections are to be registered directly with the 3D a priori data, without prior reconstruction (Fig. 3). A strategy to perform such a 2D-3D registration [10] for CT projections and a 3D mesh model has been proposed in [7]. It registers 2D projections to a 3D STL model in order to compute a variance-comparison during the CT reconstruction. The proposed method to determine the rotation can be adapted to CL and is used in our approach to work with volume data instead of mesh models.

A new algorithm solving this 2D-3D registration problem was developed and is discussed in the following. In order to register a given a priori volume, an affine transformation that consists of rotation, translation and scaling is to be applied to the laminographic data. The computation of these components will be discussed independently in the following.

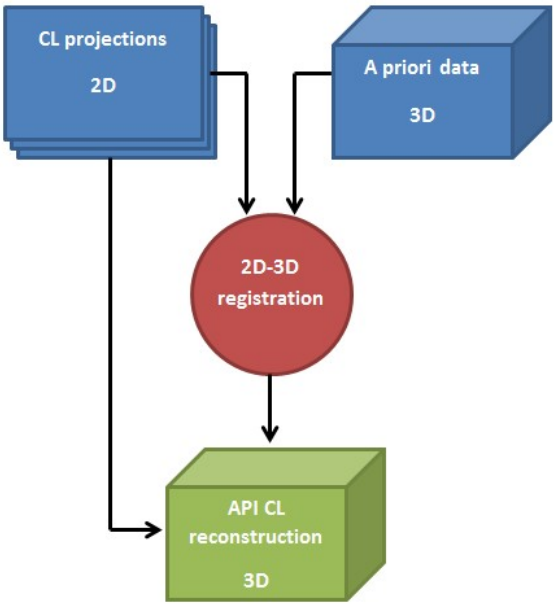

Figure 3. A priori reconstruction based on 2D-3D registration.

Although a set of measured CL data usually consists of more than a hundred projections, each corresponding to a different rotation angle of the object, only three of these projections are used in the following computations.

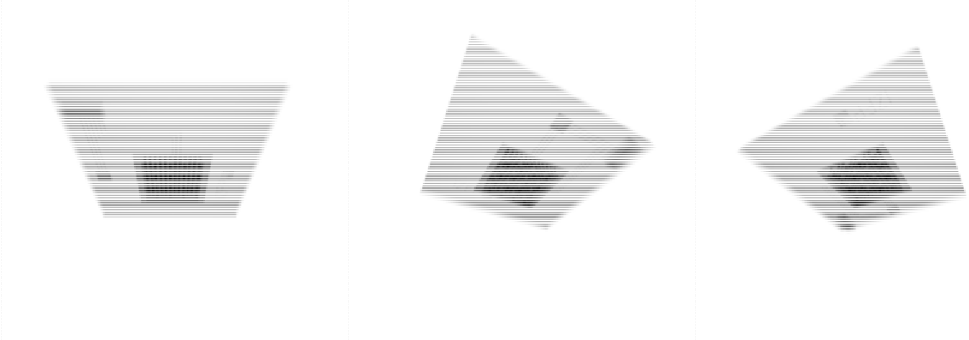

Figure 4. Reference CLARA Projections for rotation angles 0°, 120° and 240°.

In theory, the information contained in three transmission images taken from different directions is sufficient for a unique determination of all the unknowns in such an affine transformation. For greater stability and reliability of the algorithm, the angular difference of these three reference projections should be maximal, i.e. approximately 120°, as shown in an example of a circuit board in figure 4. The a priori volume of this circuit board is pictured in figure 5.

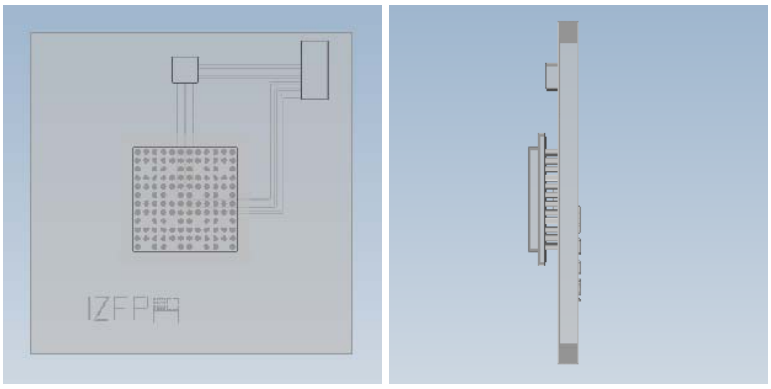

Figure 5. A priori volume, frontal and lateral view (transparent).

3.1 Rotation

In the computation of the rotation, a heuristic strategy based on systematic evaluation of rotation candidates leading to the global minimum of the evaluation function is used. Therefore, a mapping and a way of reasonably sampling the search space is found. The iterative algorithm consists of four basic steps, which will be further discussed below:

1. Sampling of the search space
2. Computation of projections of the rotated a priori volume
3. Evaluation of the projections
4. Selection of the best evaluated rotations and narrowing down the search space

3.1.1 Sampling of the search space

The initial search space is the space of all 3-D rotations D_R and can be parametrized by two angles $\theta, \varphi \in [0, \pi)$ which correspond to the spherical coordinates of the unit rotation axis and another angle $\alpha \in [0, 2\pi)$ giving the rotation angle. In order to find an equidistant sampling of rotation angles in space, the spherical angles θ and φ may not be sampled equidistantly as the transformation from spherical to Cartesian coordinates is non-linear. This transformation $P: [0, \pi)^2 \rightarrow \mathbb{R}^3$ can be written as

$$P(\theta,\varphi) = \begin{pmatrix} \sin\theta \cdot \cos\varphi \\ \sin\theta \cdot \sin\varphi \\ \cos\theta \end{pmatrix} \in \mathbb{R}^3$$

Thus, for any given grid distance $d \in \mathbb{R}$ a set $G_d \subseteq D_R$ needs to be found such that $G_d = P(M_d) = \{P(\theta,\varphi)|(\theta,\varphi) \in M_d\}$ and $M_d = \cup_{k=1,\dots,n}\ (\theta_k,\varphi_k)$ with $\Theta = \{\theta_1,\dots,\theta_n\} \subseteq [0,\pi)$ and $\Phi_k = \{\varphi_1^k,\dots,\varphi_{n_k}^k\} \subseteq [0,\pi),\ k = 1,\dots,n$. Further, for all $i = 1,\dots,n-, j = 1,\dots,n_k, \theta' \in \Theta, \varphi' \in \Phi_k$ the following conditions are to be fulfilled:

$$\|P(\theta_i,\varphi') - P(\theta_{i+1},\varphi')\| = d$$

$$\left\|P\left(\theta_i,\varphi_j^i\right) - P(\theta_i,\varphi_{j+1}^i)\right\| = d$$

Solving these equations for adequate choices of distance $d \in \mathbb{R}$ leads to step sizes

$$\Delta_\theta = \|\theta_{i+1} - \theta_i\| = \operatorname{acos}\left(\frac{2-d^2}{2}\right)$$

$$\Delta_\varphi(\theta) = \left\|\varphi_j - \varphi_{j+1}\right\| = \operatorname{acos}\left(\frac{-d^2}{2\sin^2(\theta)} + 1\right)$$

which in turns yields

$$M_d = \left\{\left(\theta_i,\varphi_j^i\right)|\theta_i = \theta_0 + (i-1)\cdot\Delta_\theta, \varphi_j^i = \varphi_0^i + (j-1)\cdot\Delta_\varphi(\theta), i = 1,\dots,n, j = 1,\dots,n_i\right\}$$

with

$$\frac{\pi}{\Delta_\varphi(\theta_i)} - 1 \le n_i < \frac{\pi}{\Delta_\varphi(\theta_i)}$$

For $\left\|\theta_i - \frac{\pi}{2}\right\|$ 'large', the step distance $\Delta_\varphi(\theta_i)$ cannot be computed from the formula above as $\frac{-d^2}{2\sin^2(\theta)} + 1 > 1$. In this case, we set $\Phi_k = \{\varphi_0^k\}$.
The sampling of the rotation angles is straightforward and given by

$N_d = \{\alpha_0 + (i-1)\cdot d|\ i = 1,\dots,m\}$, with $\frac{2\pi}{d} - 1 \le m < \frac{2\pi}{d}, m \in \mathbb{N}$.

The equidistant sampling of the parameter space D_R is then given by $P_d = M_d \times N_d$.

3.1.2 Computation of projections of the rotated a priori Volume

After having found a search space sampling the elements of that set need to be evaluated. In order to be able to do so, comparable data needs to be obtained. Therefore, three projections of the rotated a priori volume are to be computed. If the proper geometry information is used in these computations, the resulting projections can be compared to the three corresponding measured projections in order to find an evaluation for the rotation applied. The size and resolution of the projections to be created is chosen according to the originally measured CL data (i.e. original number of voxels multiplied by $(2^n)^2$, original voxel size multiplied by 2^{-n} for any $n \in \mathbb{N}$).

The geometry data which needs to be plugged in is determined by the geometrical setup of the laminographic scanner used. Instead of applying the rotation to the given a priori Volume (3D), the rotation can be applied to the set of geometry data. For each

measured projection, this data file contains the positions of the X-Ray source, the detector and its spanning vectors in 3-D space. Obviously, the computational effort in rotating the geometry data is significantly smaller than that in rotating a 3-D volume which may be made up of millions of voxels. Further, if rotating the discrete a priori volume, interpolating voxel values is inevitable leading to further losses of accuracy.

Having rotated the given geometry data the projections can be computed by simulating one X-ray for each detector pixel to be evaluated. Therefore, for each volume voxel hit by the ray, a ray weight corresponding to the ray's relative length within that voxel needs to be computed such that all the weights add up to unity. Note that the volume's center is positioned in the origin just as it is in the SART reconstruction process. To find the pixel value corresponding to the detector pixel, the weighted sum of all voxels hit is computed.

3.1.3 Evaluation of the simulated projections

Finding a reasonable evaluation value is challenging since the grey values of the projection pairs cannot be compared directly because of the different image acquisition methods. Comparability can be achieved by binarization (or trinarization) of the projections, i.e. segmentation in 2 or 3 different areas. In order to segment a projection into two areas, distinguishing between pixels that where hit by X-rays either having passed any material on their way from source to detector or not, a single threshold is used. This threshold is found in a way similar to Otsu's method [5]. Otsu starts with computing the variances of the two classes the image is divided into by a threshold $T \in \mathbb{N}$. The 'ideal' threshold is selected as the one minimizing the intra-class variances, or, completely equivalent, maximizing the between-class variance. Let $\omega(T)$ be the probability of the 'material class' (consisting of all pixels with grey value $< T$), $\mu_0(T)$ and $\mu_1(T)$ the means of the material and the 'air class' and μ the whole projections' mean. The between class variance, which is minimized in Otsu's method, is given by

$$\sigma^2(T) = \omega(t)(\mu_0(T) - \mu)^2 + (1 - \omega(t))(\mu_1(T) - \mu)^c \qquad (3)$$

with $c = 2$. In the algorithm introduced here, the parameter c is chosen greater than 2 resulting in a higher weight on a small intra-class variance of the air class than on a small intra-class variance of the material class. This is reasonable as the air class is to consist only of pixels that where hit by X-rays not having crossed any material and therefore having been hardly attenuated on their path. Thus the variance of grey-values within this class should be very small, whereas the variance within the material class may be significantly higher. In some cases, distinguishing a third projection segment allowing for more distinguishable evaluations can be necessary. Therefore, a third class of pixels, containing those that were hit by very strongly attenuated X-rays and therefore corresponding to denser material, is defined. To accomplish such a distinction, another binarization using a single threshold is performed on the material class. In this case, the threshold is found by computing a specified quantile of the material class's pixel values. As the translation is not known yet, the objects can be positioned differently within the projection pairs. To compensate for this, object barycenters are computed by averaging over all border pixels of the material class and the resulting real-valued pixel indices are moved to the projection center. Once the preprocessing is completed, the rotation's evaluation value can be computed as

$$\Delta(d) = \frac{1}{3}\sum_{i=1}^{3}\frac{1000}{n^2}\sum_{j=1}^{n}\sum_{k=1}^{n}\left((p_i^R)_{(j,k)} - \left(p_i^E(t)\right)_{(j,k)}\right)^2 \quad (4)$$

where p^R are the centered CL projections and $p^E(t)$ the centered simulated projections for rotation $t \in D_R$.

3.1.4 Selection of the best rotations and narrowing down the search space

To find the ideal rotation, an iterative approach is used. After having evaluated all rotations of the first equidistant rotation set, the best or a number of best rotations are selected. When doing so only local minima of the initial set may be picked and the number of rotations picked is indirectly determined by a user-input parameter δ_1. This value determines up to which relative deviation from the best evaluation value obtained so far (Δ_{max}^i where $i \in \mathbb{N}$ is the number of iterations already performed) rotations may be selected as candidates for the next iteration. Thus, a rotation $r_i \in D_R$ may only be selected if

$$\left\|\frac{\Delta(r_i)-\Delta_{max}^i}{\Delta_{max}^i}\right\| < \delta_i \quad (5)$$

holds true. Around each selected rotation, a refined equidistant grid of rotations that are to be evaluated in the following iteration is computed. The size of that grid, i.e. the number of grid elements and the factor by which the grid spacing is downscaled, can also be determined by the user. In the following iterations, several independent grids are considered. The grid sizes should be chosen in such a way that the grids cannot overlap and each grid leads to a different local minimum. This procedure is repeated until the grid spacing falls below a certain threshold and thus, the local minima are approximated sufficiently exactly. As the evaluation mapping $\Delta: D_R \rightarrow \mathbb{R}$ is not convex and may have a large number of local minima, such an iterative procedure tracking different local minima is necessary in order to find the global minimum. Still, this is only possible if grid distance in the initial set of rotations is sufficiently small. In some cases, especially in case of binary a priori data, an initial rotation allowing for convergence against the unique global minimum may be inevitable.

3.2 Translation

The three-dimensional translation vector is computed after scaling and rotation have already been found, thus one can assume three pairs of projections showing the object in identical orientations. For each projection an image barycenter is computed and, by subtraction, a two-dimensional translation is found for each pair of projections as illustrated in figure 6.

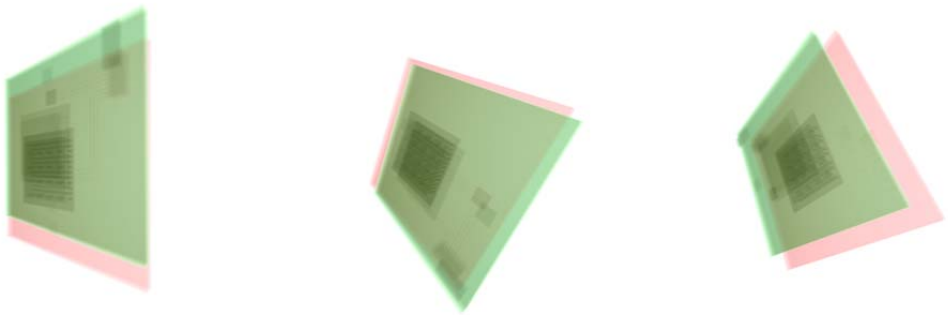

Figure 6. Pairs of projections, red measured CL data, green simulated projections.

One can compute corresponding 3D translations $t_i, i = 1,2,3$ within the detector plane as the detector orientation for each rotation angle is known from the CL measurement's geometry data. These translations are projections of the actual object translation $x \in \mathbb{R}^3$ onto the detector plane in respective X-ray directions. Thus, it holds for $i = 1,2,3$

$$x = \frac{1}{f} \cdot t_i + \lambda_i \cdot s_i \qquad (6)$$

with $f \epsilon \mathbb{R}$ the geometry-dependent magnification factor, $t_i \in \mathbb{R}^3$ the translation vectors computed from projection pairs and geometry, $s_i \in \mathbb{R}^3$ the X-ray transmission direction through the simulated projection's barycenter and real numbers $\lambda_i \in \mathbb{R}$, $i = 1,2,3$. Due to small variations in the object's actual magnification depending on its exact (unknown) position, this formula is not completely accurate. The translation x can be found by solving the optimization problem

$$\underset{x}{\operatorname{argmin}} \left(\min_{\lambda \in \mathbb{R}^3} \left(\sum_{i=1}^{3} \left\| \left(\frac{1}{f} \cdot t_i + \lambda_i \cdot s_i \right) - x \right\|^2 \right) \right) \qquad (7)$$

Computation of this convex function's gradient and setting it equal to zero yields a linear system of six equations. The translation allowing for registration of a priori and CL data is then obtained by solving this system.

3.3 Scaling

In many cases, a computation of a scaling factor is not necessary as it is already known or may be solved in a preprocessing step. The method described here for finding the scaling factor is not very exact and should not be used if high accuracy is required. Nevertheless, application of the method for differently scaled datasets allows for quite accurate computation of rotation and translation which is not possible without roughly determining the scaling factor to be applied.

Similarly to the rotations' algorithm, a scaling factor can be estimated from the bi-/trinarized projection sets. By summing up all foreground pixels (values 1 and 2) the projection's object area can be computed. Comparing the summed up object areas of the two sets of three projections to each other gives an estimation for the scaling factor's square. The estimation is better, the more similar the object orientation in the projection pairs, i.e. the smaller the evaluation value Δ. Still, caused by the two different image acquisition methods used, the scaling factor cannot be computed exactly even if the object orientations are completely conform. If available, other means of determining the scaling factor are to be preferred.

4. Results & Discussion

4.1 Simulated data

To validate the algorithm, simulated data of a circuit board with a fracture is used. The projections were simulated using CLARA geometry; a voxel volume containing a defect free version of the circuit board was computed by the simulation software Scorpius XLab

and was used as a priori model. The a priori volume was consecutively rotated by -26° around the x-axis, 40° around the y-axis and 72° around the z-axis which is equivalent to a single rotation of 76.38° around the axis (-0.5934, 0.2351, 0.7698). An additional translation by the vector (-1.0,-1.4,-0.8) was applied. This information is used to easily determine the algorithm's accuracy.

Table 1 summarizes the parameters of translation and rotation which were computed using the 2D-3D registration algorithm and compares these values to the actual transformation applied to the a priori volume. The computed rotation angles deviate by less than 0.0015% from the ground truth. For the translation vector, the maximal deviation is 3.4 % for the z-component, and less for the other two components (0.81% and 0.58%). The accuracy depends on the bi- and trinarization thresholds which are applied to the projection sets to be compared. At the same time, precision can be increased by using larger projections due to the greater number of pixels contained.

Table 1. Difference between computed and actual transformation parameters

Axis	Translation computed [cm]	Translation [cm]	Rotation computed [°]	Rotation [°]
x	-1.0081	-1.0	-26.0038	-26.0
y	-1.4081	-1.4	40.0005	40.0
z	-0.8275	-0.8	71.9911	72.0

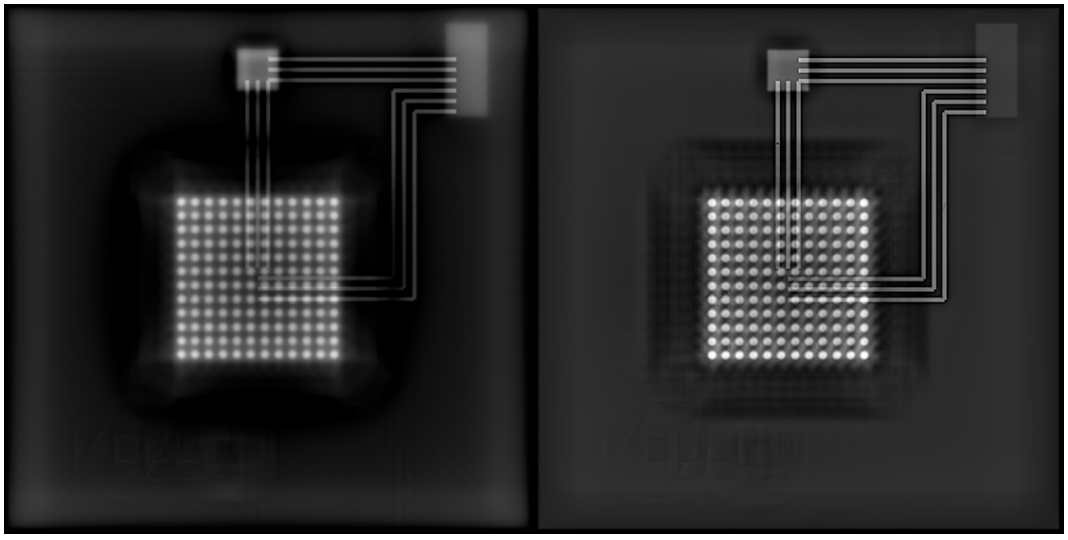

Figure 7. Circuit board phantom, frontal view, left SART, right AP-SART using a registered a priori volume.

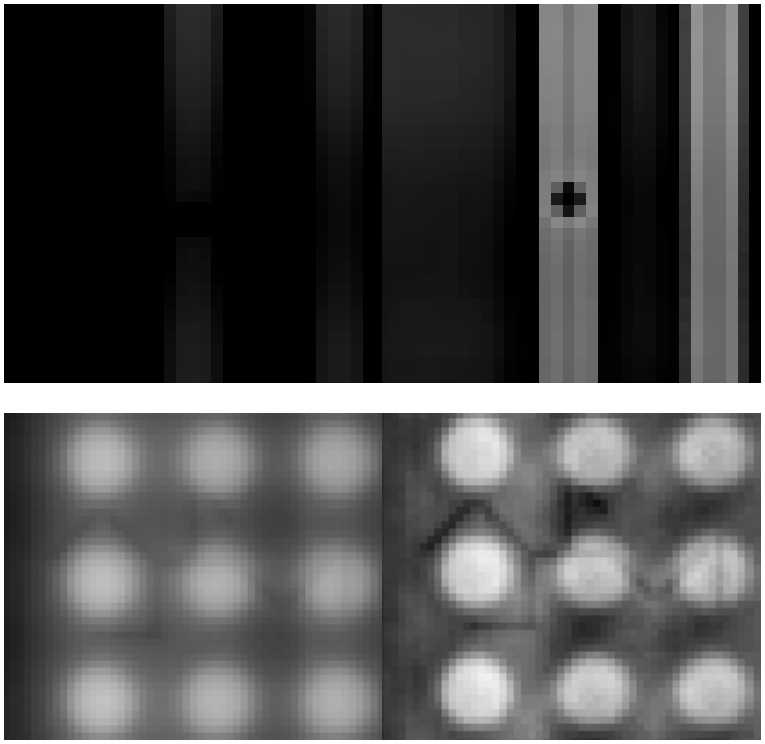

Figure 8. Circuit board phantom, frontal view, magnified, left SART, right AP-SART using a registered a priori volume.

The gain in quality that can be achieved by the use of registered a priori information is illustrated in a few figures: In the reconstruction's frontal views shown in figure 7 and 8 the defect, a branched crack, is clearly better visible when registered a priori information is used. Figure 9 shows the lateral views of the reconstructed volumes. The images demonstrate that the blurring artefacts can be drastically reduced by the use of a priori information. While the circuit board's contours cannot be recognized in the traditional reconstruction, the a priori reconstruction not only shows the edges sharply but also allows the defects to be detected. In this lateral view the crack within the circuit board's base consists of two branches and thus is visible as two porosities in the magnified AP-SART reconstruction, which cannot be discerned in the normal SART reconstruction without a priori information.

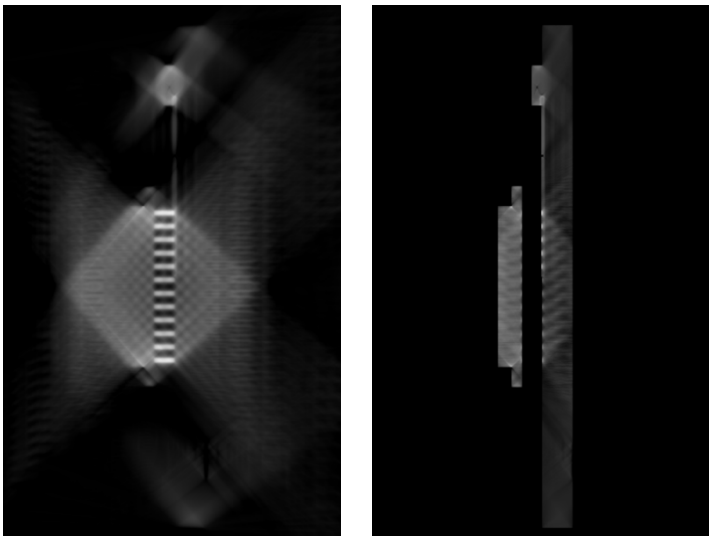

Figure 9. Circuit board phantom, lateral view, left SART, right AP-SART using registered a priori volume.

4.2. Measured data

A test on measured data without known orientation was also performed. A fiber reinforced plastics T-profile was scanned with CLARA and a conventional CT scanner. An a priori volume of the entire object was computed using the reconstruction of the CT data. To this end, the CT reconstruction volume of 510 x 640 x 1024 voxels was binarized into air (g_j= 0) and material (g_j= 1) areas. All air voxels inside the object were set to 1 also, to guarantee that no information about the object's interior from the CT scan was used as a priori information. 400 projections of 2048^2 pixels were measured and used to do a standard SART and an AP-SART reconstruction of a volume of 510 x 640 x 1024 voxels. The registration between the orientation of the a priori volume from the CT scanner and the projections from CLARA was computed using the proposed algorithm.

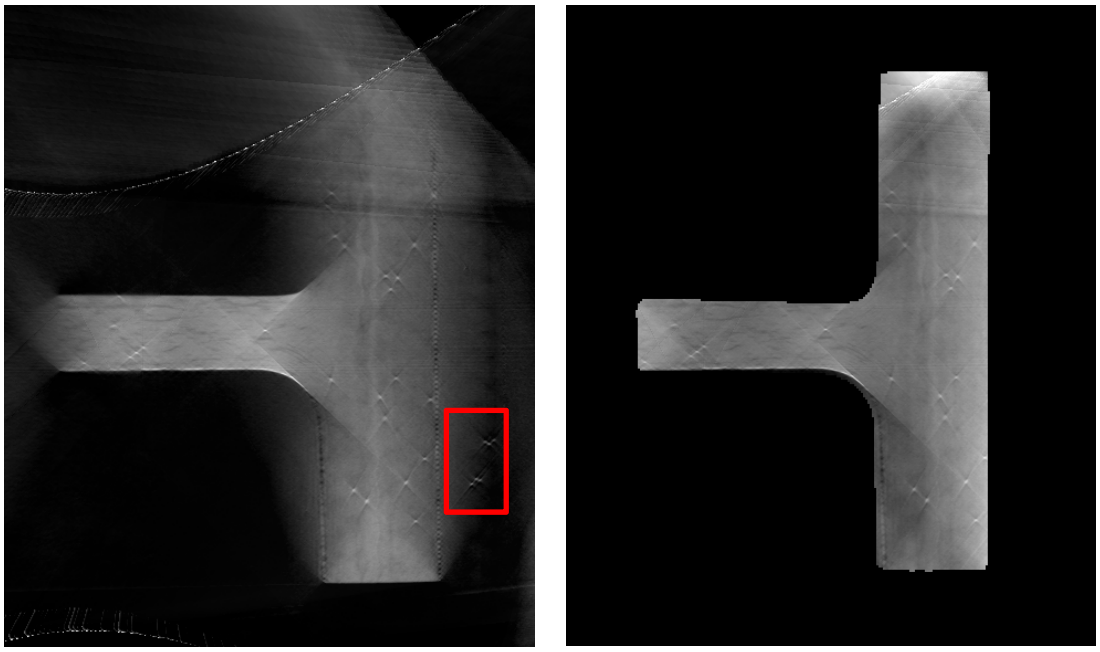

Figure 10. T-profile, lateral view, left SART, right AP-SART using registered a priori volume.

The standard SART reconstruction without additional knowledge (fig. 9 left) shows typical laminography artefacts which blur the shape of the object. There are also some fiber cross sections (small white points) falsely reconstructed in the air area (red box), where there clearly is no object. The AP-SART (fig. 9 right) result with registered a priori information on the other hand reconstructs the object's form faithfully and significantly reduces the laminography artefacts. The fiber cross sections are also rendered clearly. The gray level difference in the upper and lower parts of the object are due to the laminographic geometry which cannot reconstruct the absolute density values faithfully, but which poses no problem for the identification of the fibers.

5. Conclusion

The use of a priori information in the reconstruction of laminographic measurement data can dramatically increase the quality of the resulting volume and thus enables the detection of defects which cannot be identified within the traditionally reconstructed volume. The algorithm presented in this work successfully registers 2D CL data with 3D a priori models and therefore allows for an effective use of given a priori knowledge in the SART reconstruction process. Apart from its benefits for computed laminography this technique is also very useful for classic CT, for instance reducing the number of projections needed for sufficient reconstruction quality and thereby minimizing the measurement and reconstruction time or for dealing with limited angle datasets.

Funding: This work was partially funded by the DFG in the project "Parallel Iterative Methods with A Priori Information for Robust Computed Laminography of Low Contrast, Difficult-To-Measure Objects" MA 5836/1-1.

References

[1] Maisl M, Porsch F, Schorr C. Computed Laminography for X-ray Inspection of Lightweight Constructions, International Symposium on NDT in Aerospace. Berlin : Deutsche Gesellschaft für zerstörungsfreie Prüfung (DGZfP), 2010 (DGZfP-Berichtsbände 124)

[2] Andersen A, Kak A. Simultaneous algebraic reconstruction technique (SART): a superior implementation of the art algorithm. Ultrason Imaging 1984, 6(1):81–94

[3] Schorr C, Maisl M. Exploitation of geometric a priori knowledge for limited data reconstruction in non-destructive testing, Proceedings of the Fully3D Conference 2013, pp 114-117

[4] Schorr C, Maisl M. A ray-length-based ROI-correction for computed laminography, Proceedings of 5th Conference on Industrial Computed Tomography 2014, pp. 253-258

[5] Otsu N. A threshold selection method from gray-level histograms. Automatica 1975, 11(285-296):23-27

[6] Gottesfeld Brown L. A survey of image registration techniques. ACM computing surveys (CSUR) 1992, 24(4):325-376

[7] Franz M. EAR - Einsatzsynchrone Artefakt Reduktion. PhD thesis, Friedrich-Alexander-Universität Erlangen-Nürnberg, 2009.

[8] Zitova B, Flusser J. Image registration methods: a survey. Image and vision computing 2003, 21(11):977-1000

[9] Bellekens B, Spruyt V. Maarten Weyn, RB. A survey of rigid 3D pointcloud registration algorithms. Fourth International Conference on Ambient Computing, Applications, Services and Technologies 2014, Proceedings (pp. 8–13)

[10] Markelj P, Tomaževič D, Likar B, Pernuš F. A review of 3D/2D registration methods for image-guided interventions, Med Image Anal. 2012 Apr;16(3):642-61

[11] Feldkamp LA, Davis LC, Kress JW. Practical cone-beam algorithm. J. Opt. So. Am. A 1984, 1(6):612-619